ELSEVIER

Journal of Nuclear Materials 254 (1998) 234–242

journal of nuclear materials

Effect of additives (Cr_2O_3, Al_2O_3, SiO_2, MgO) on diffusional release of ^{133}Xe from UO_2 fuels

S. Kashibe *, K. Une

Nippon Nuclear Fuel Development Co., Ltd., 2163, Narita-cho, Oarai-machi, Higashi-ibaraki-gun, Ibaraki-ken 311-1313, Japan

Received 7 April 1997; accepted 14 November 1997

Abstract

The effect of small amounts of additives on the diffusional release of ^{133}Xe from UO_2 fuel has been examined in the temperature range of 1100–1600°C by means of a post-irradiation annealing technique. The fuel specimens were lightly irradiated to 4 MWd/tU in JRR-4 reactor. Four kinds of additives, i.e. 0.065 wt% Cr_2O_3, 0.076 wt% Al_2O_3, 0.085 wt% SiO_2 and 0.50 wt% MgO, were used. The Cr_2O_3, SiO_2 and MgO dissolved in the UO_2 matrix; their dissolved concentrations were 0.012, 0.045 and 0.08 wt%, respectively. The diffusion coefficient of ^{133}Xe for the Cr_2O_3-doped UO_2 was about three times larger than that for the undoped UO_2 at high temperatures of 1500–1600°C, while the value for the SiO_2-doped UO_2 was about one order of magnitude smaller than that for the undoped UO_2 over the whole temperature range. The diffusional fission gas release was not affected by the addition of MgO, although MgO in the matrix was partly present as a large number of small MgO precipitates of 9 nm uniformly dispersed in it. The added Al_2O_3, which did not dissolve in the matrix, had no effect on the diffusion coefficient. The effect of the soluble additives on fission gas diffusion was discussed in terms of the lattice defect equilibrium model. © 1998 Elsevier Science B.V.

1. Introduction

The release of the fission gases (xenon and krypton) in a reactor fuel pin is an important performance-limiting factor. For this reason the diffusion characteristics of rare gases in UO_2 have been the subject of extensive research. Lawrence [1] and Matzke [2] have reviewed the data on fission gas diffusion in UO_2 and discussed its mechanism. Both these workers pointed out that the diffusion coefficient is significantly affected by the stoichiometry (O/U ratio) or the defect structure of UO_2. The defect structure of UO_2 is changed by not only the O/U ratio, but also by the presence of foreign cations with various valences. Therefore, many kinds of impurities in UO_2 pellets may affect the diffusion coefficient. Recently, small amounts of additives are intended to be mixed with UO_2, in order to improve sinterability or to obtain large-grained pellets. For the former purpose alumino-silicate (Al_2O_3–SiO_2) has been adopted [3], while for the latter purpose Nb_2O_5 [4–8], TiO_2 [4,9], Cr_2O_3 [10] and MgO [11–13] have been chosen.

There have been several post-irradiation annealing experiments [10,14,15] to study the effect of additives on the diffusion coefficient of fission gases. But one controversial subject remains for study: no change of the diffusion coefficient was found for 0.8–1.2 wt% Y_2O_3-, La_2O_3-, ZrO_2- and Nb_2O_5-doped UO_2 [14] and 0.5 wt% Cr_2O_3–UO_2 [10], although the diffusion coefficient of ^{133}Xe was reported to be remarkably enhanced by the doping of 0.2 wt% TiO_2 or 0.5 wt% Nb_2O_5 into UO_2 in the experiments using lightly irradiated specimens (burnup: 4 MWd/tU) [15]. Moreover, a subsequent experiment showed that this enhancement effect by the addition of Nb_2O_5 or TiO_2 was still valid after irradiation at 23 GWd/tU [16]. Besides these annealing tests, analyses of the fission gas release data for 0.5 wt% Cr_2O_3–UO_2 pellet (1.4–4.5 GWd/tU) [10] and 0.75 wt% MgO–UO_2 pellet (28 GWd/tU) [11]

* Corresponding author. Tel.: +81-29 266 2131; fax: +81-29 266 2589; e-mail: kashibe@nfd.co.jp.

PII S0022-3115(97)00356-5

indicated no effect of the additive for the former, but suggested a suppression effect on the diffusion coefficient for the latter. The decreased diffusivity in the $MgO–UO_2$ pellet was assumed to be ascribed to a trapping effect of fission gases by small MgO precipitates in the grains.

In this study, the effect of small amounts of additives (0.065 wt% Cr_2O_3, 0.076 wt% Al_2O_3, 0.085 wt% SiO_2 and 0.50 wt% MgO) on the diffusion coefficient of ^{133}Xe, which was not investigated in the previous study [15], was examined in the temperature range of 1100–1600°C for lightly irradiated specimens, using a post-irradiation annealing technique.

2. Experimental

2.1. Specimens

Five types of fuel pellets were prepared from one lot of natural UO_2 powder, which had the following impurity levels. Fe: <13 ppm, Cr: <2 ppm, Al: 2 ppm, Si: <6 ppm and Mg: <1 ppm. As additives, four kinds of oxide powders of Cr_2O_3, Al_2O_3, SiO_2 and MgO (purity: $\geqslant$ 99.9–99.999%) were chosen. The powder compacts of undoped (as a reference) and additive-doped UO_2 were obtained as follows. The UO_2 powder containing no binder was mixed with weighed amounts of additive oxide powder in an agate mortar during 1 h. The undoped and additive-mixed UO_2 powders were pressed under pressures of 180–220 MPa. The compacts were sintered under two different conditions. The undoped and (Cr_2O_3, Al_2O_3 or SiO_2)-mixed UO_2 compacts were sintered in hydrogen at 1750°C for 2 h. On the other hand, the MgO-mixed UO_2 compact was sintered in argon at 1660°C for 2 h to form a $(U, Mg)O_2$ solid solution with good homogeneity. Then it was annealed in a slightly oxidizing atmosphere of wet $N_2 + 8\%H_2$ (dew point: 20°C) at 1660°C for 2 h and finally, in a reducing atmosphere of dry $N_2 + 8\%H_2$ (dew point: -35°C) at 1660°C for 2 h to precipitate MgO particles of nanometer size in the UO_2 matrix. This two-step annealing was adopted to prevent the formation of microcracks due to the precipitation of MgO and/or lattice parameter non-uniformity in the sintered pellets caused by a rapid reduction.

Table 2
Results of chemical analyses and fractional retention of additive in each type pellet

Fuel pellet	Metallic concentration (ppm/U)						Fractional retention (%)
	Fe	Ni	Cr	Al	Si	Mg	
Undoped	<5	<7	<5	<10	<5	<10	—
Cr_2O_3-doped	10	<7	239	<10	32	<10	47
Al_2O_3-doped	10	<7	<5	121	26	<10	27
SiO_2-doped	14	<7	<5	19	370	<10	82
MgO-doped	<10	<10	<10	<10	25	3300	96

The nominal concentration of each additive oxide, and the grain size and density of the sintered pellets are summarized in Table 1. The contents of Cr_2O_3, Al_2O_3 and SiO_2 additives were low levels of 0.065, 0.076 and 0.085 wt%, respectively. The grain sizes for the Al_2O_3- and $MgO–UO_2$ pellets were 26–30 μm, being about double those (13–17 μm) for the other pellets. The sintered densities measured by the immersion method using *meta*-xylene were 10.46 g/cm^3 (95.4% TD) for the $MgO–UO_2$ pellet and 10.71–10.75 g/cm^3 (97.7–98.1% TD) for the others. The evaluation procedure of the dissolved concentration of additive oxides in Table 1 is described later.

Some amount of the additive oxide must escape from the pellets during the sintering and annealing processes. Therefore, conventional chemical analyses of inductively coupled plasma emission spectrochemical analysis (Ni and Al), absorption spectrometry (Fe, Si and Cr) and atomic absorption spectrometry (Mg) were made for each pellet. The detection limits of these analyses are 5–10 ppm based on uranium metal. The results are summarized in Table 2 in metallic content (ppm). The concentrations of Si (25–32 ppm) in the (Cr_2O_3, Al_2O_3 or MgO)-doped UO_2 pellets were higher than that (5 ppm) in the undoped UO_2 pellet. This is attributable to Si contamination during the mixing process of UO_2 and additive oxide powders, since the major component of the agate mortar is SiO_2. There was no cross contamination of additives from the fact that the amounts of metallic elements, except for Si, in the additive-doped pellets were almost the same as those in the undoped pellet. Based on the results of chemical analyses,

Table 1
Nominal and dissolved concentrations of additive oxides, grain size and density of each type pellet

Fuel pellet	Nominal concentration (wt%)	Grain size (μm)	Density (g/cm^3)	Dissolved concentration[a] (wt%)
Undoped	–	15	10.71	–
Cr_2O_3-doped	0.065	15	10.73	0.012
Al_2O_3-doped	0.076	30	10.75	–
SiO_2-doped	0.085	17	10.75	0.045
MgO-doped	0.50	26	10.46	0.080

[a]Estimated from chemical analyses and EPMA examinations.

Table 3
Specific surface area, O/M ratio and equivalent sphere radius for each type specimen

Series	Fuel specimen	Specific surface area (m^2/g)	O/M ratio	Equivalent sphere radius (μm)
I	undoped	0.146	2.004	1.88
	Cr_2O_3-doped	0.168	2.002	1.63
	Al_2O_3-doped	0.158	2.002	1.73
	SiO_2-doped	0.214	2.002	1.28
II	undoped	0.073	2.001	3.75
	MgO-doped	0.073	1.999	3.75

the fractional retentions of additives in the pellets were calculated and are also listed in Table 2. They were 27% for the Al_2O_3–UO_2 pellet and 47% for the Cr_2O_3–UO_2 pellet, indicating that more than the half of these additives were released from the pellets during sintering. The lower fractional retention of Al_2O_3 is possibly related to the eutectic reactions of UO_2–Al_2O_3 and/or UO_2–Al_2O_3-impurity SiO_2. By contrast, the fractional retentions were 82% for the SiO_2–UO_2 pellet and 96% for the MgO–UO_2 pellet.

The five types of sintered pellets were crushed in an agate mortar and sieved to about 20 μm mesh size. The fine powders attached on the sieved powders were removed by ultrasonic cleaning in acetone. Before irradiation, the powders were annealed in H_2 at 1000°C for 3 h, in order to control the O/M ratio to 2.00 and to anneal defects which had been introduced into the powders during crushing. The specific surface area for sieved and annealed samples from sintered pellets was determined by the BET method using krypton gas. The O/U ratio for these samples was determined by conventional polarography with an accuracy of ± 0.001.

The specific surface area and O/M ratio for the five specimens are given in Table 3. The equivalent sphere radius calculated by Eq. (1) for archive specimens is also shown there. Booth's equivalent sphere radius, *a*, is expressed as

$$a = 3/Sd, \tag{1}$$

where *S* is the specific surface area and *d*, the bulk density of the specimens. In this study, two series of experiments were carried out, using specimens with different specific surface areas, which resulted from different acetone cleaning times of the sieved powders regarding attached fine powders. The contamination of the attached fine powders remarkably influences the value of specific surface area. In series I, the Cr_2O_3-, Al_2O_3- and SiO_2–UO_2 specimens and the undoped UO_2 specimen were tested. Their specific surface areas were 0.146–0.214 m^2/g (equivalent sphere radius: 1.88–1.28 μm). In series II, the MgO–UO_2 and undoped UO_2 specimens, which had a different specific surface area of 0.073 m^2/g (3.75 μm), were used. The mean equivalent sphere radii for series I and II experiments were 1.5 and 3.8 μm, respectively. The O/M ratios for the present specimens ranged from 1.999–2.004 (Table 3) were close to the stoichiometric composition. Only the lattice parameter of the MgO–UO_2 pellet was measured by X-ray diffractometry, in order to evaluate the dissolved MgO concentration in the UO_2 matrix. It was 0.5468 nm, which agrees with the value of the stoichiometric (U, Mg)O_2 solid solution with dissolved MgO concentration being 0.08 wt% [17].

2.2. Irradiation conditions

The fuel samples (about 10 mg each) of sieved and annealed powders were irradiated in evacuated quartz capsules for 6 h at a thermal neutron flux of 5×10^{17} $n/m^2/s$ in the JRR-4 reactor of JAERI, giving the total dose of 1×10^{23} fissions/m^3 (4 MWd/tU). The temperature inside the capsule during the irradiation was not measured, but could be estimated as lower than 100°C [18]. After irradiation, the specimens were cooled for a period of 8–13 d to let the short-lived nuclides decay.

2.3. Annealing experiments

The Mo capsule containing the irradiated specimen was heated by induction furnace in a stepwise pattern from 1100–1600°C (heating rate: 1.7°C/s; temperature step: 100°C; holding time: 1 h). Sweep gas was a high purity He + 2%H_2 mixture at a flow rate of 60 cm^3/min. The β-activity (energy: 346 keV, half-life: 5.27 d) of released ^{133}Xe during heating was continuously measured with an ionization chamber. After the annealing experiments, the residual ^{133}Xe in the specimen was determined after dissolving the powder in hot nitric acid.

3. Results

3.1. EPMA, SEM and TEM examinations

The additive oxides used in this study are known to have low or no solubility in UO_2 [19]. In fact, large precipitates of 1–5 μm in size are observed in all the

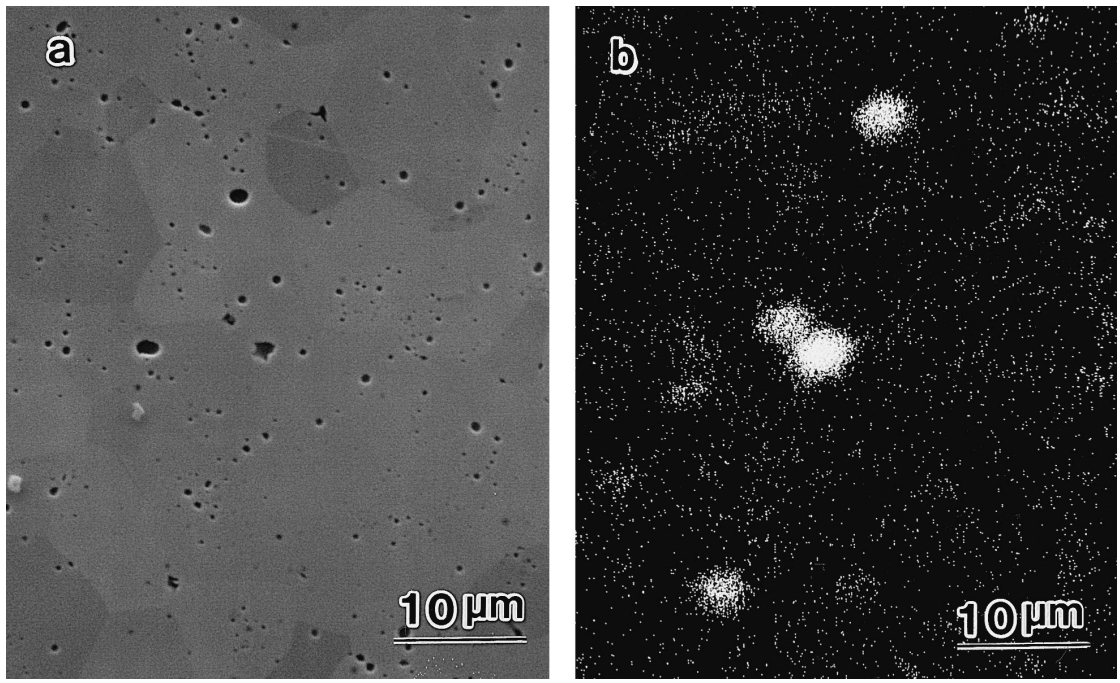

Fig. 1. (a) Scanning electron micrograph and (b) characteristic X-ray image of Si for SiO_2-doped pellet on polished surface.

additive-doped pellets. As way of example, a scanning electron micrograph (SEM) and a characteristic X-ray image for the polished surface of SiO_2–UO_2 pellet are shown in Fig. 1. The large precipitates are present in as-fabricated pores on grain boundaries. Therefore, the additive concentrations (Table 2) measured by chemical analyses are those for the additives distributed between the large precipitates and the UO_2 matrix. In the matrix, the additives are present as solution and/or small precipitates. The additive concentration in the matrix was measured by EPMA. Fig. 2 gives typical characteristic X-ray spectra of Si and Al in their doped pellets. A significantly high Si–$K_{\alpha 1}$ peak is observed for the former, but Al–$K_{\alpha 1}$ peak is lacking for the latter, indicating that no Al is present in the matrix. The presence of Cr_2O_3 and MgO in the pellets was confirmed. The matrix concentrations obtained by

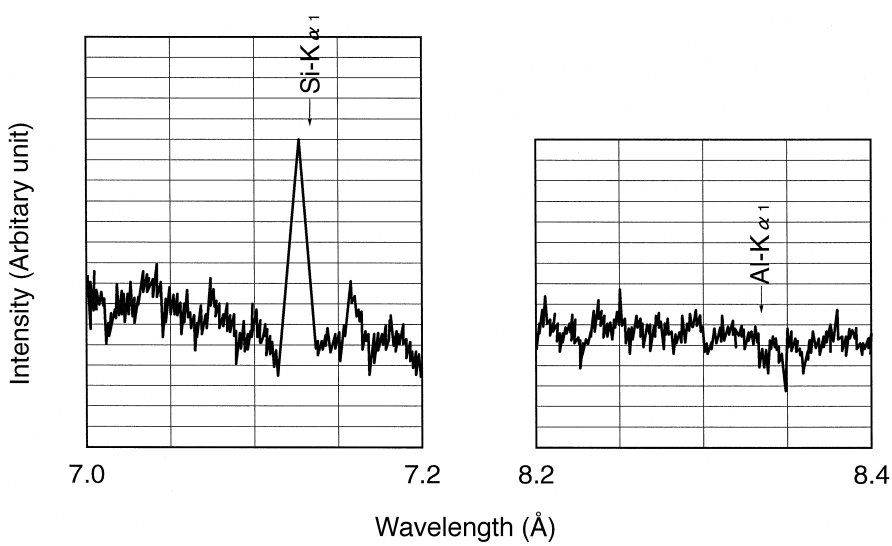

Fig. 2. Characteristic X-ray spectra of Si and Al in their respectively doped pellets.

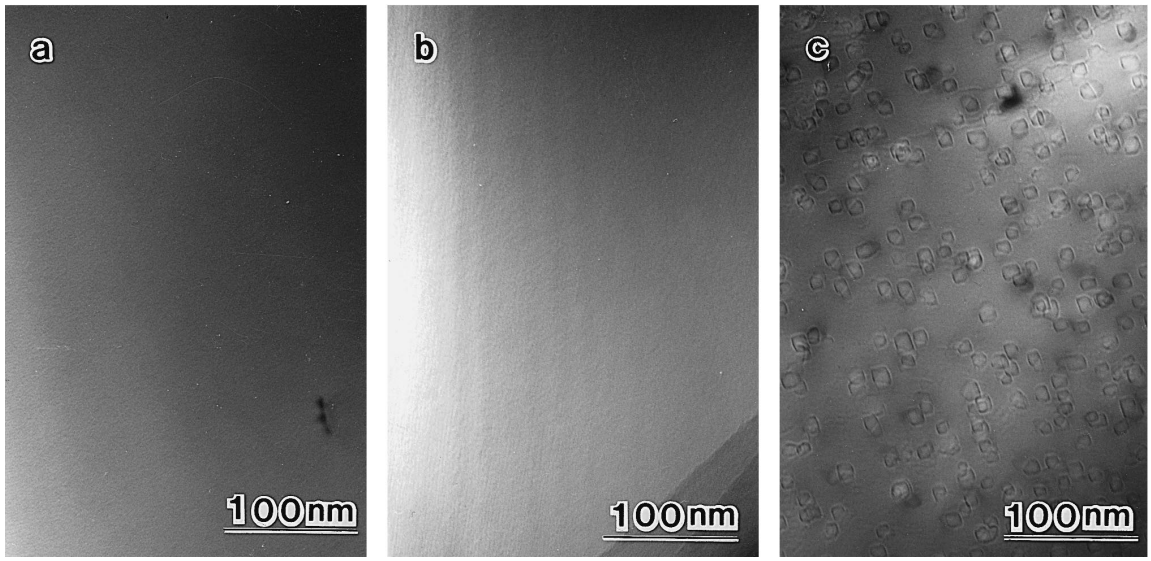

Fig. 3. Bright-field transmission electron micrographs of additive-doped pellets: (a) Cr_2O_3–UO_2; (b) SiO_2–UO_2 and (c) MgO–UO_2.

EPMA are 0.012 wt% for Cr_2O_3, 0.045 wt% for SiO_2, 0.46 wt% for MgO and below the detection limit (< 0.008 wt%) for Al_2O_3.

Next, observation of the microstructure with a transmission electron microscope (TEM) was carried out for the additive (Cr_2O_3, SiO_2 or MgO)-doped pellets, in order to examine the presence of small precipitates in the matrix. Fig. 3(a)–(c) reproduce their high magnification TEM images. For the Cr_2O_3- and SiO_2–UO_2 pellets, no precipitates larger than 1 nm are found in the matrix. Namely, Cr and Si at the aforementioned matrix concentrations are concluded to be dissolved. For the MgO–UO_2, many small precipitates (average size: 9 nm) are found and they are homogeneously distributed with a density of 3×10^{22} m^{-3}. The small MgO precipitates were formed during the two-step annealing at 1660°C in the slightly oxidizing atmosphere of $N_2 + 8\%$ H_2 (dew point: 20°C) followed by in the reducing atmosphere of $N_2 + 8\%$ H_2 (dew point: -35°C). Fig. 4 shows a lattice image of the MgO–UO_2 specimen before irradiation. No precipitates smaller than 9 nm are found in the matrix. Assuming that the MgO precipitates are spherical with radius R, the weight percent of the precipitates is given by

$$W = 4\pi R^3 N \rho_M / 3\rho_U \times 100, \quad (2)$$

where N is the number density of the precipitate (m^{-3}) and ρ_M and ρ_U are the densities (kg/m^3) of MgO and UO_2, respectively. In this specimen, the concentration of small MgO precipitates is calculated to be 0.38 wt%. Then, the concentration of dissolved MgO, which corresponds to the difference between the amounts of retained MgO in the pellet (0.46 wt%) and precipitated MgO (0.38 wt%), is 0.08 wt%. This dissolved MgO concentration is in good agreement with the result obtained from the measured lattice parameter (0.5468 nm), using the reported correlation between the lattice parameter and MgO concentration in a stoichiometric (U, Mg)O_2 solid solution [17]. The dissolved concentrations of additive oxides are listed in the last column of Table 1, together with the nominal additive concentrations.

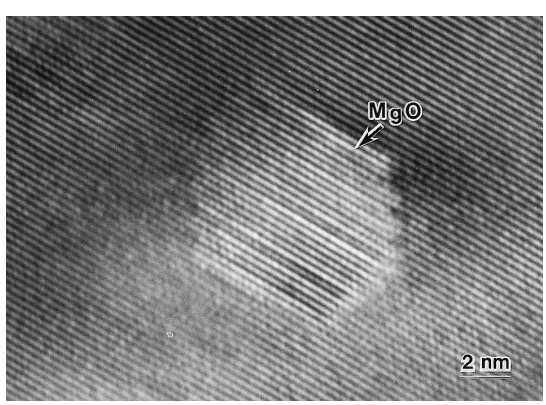

Fig. 4. Lattice image of MgO–UO_2 specimen before irradiation.

3.2. ^{133}Xe release

In the post-irradiation annealing experiments, the cumulative fractional release, F, can be related to the equivalent sphere radius, a, by the following approximation ($F \leqslant 0.3$) of Booth's model:

$$F = (6/a)(Dt/\pi)^{1/2}, \quad (3)$$

where D is the effective diffusion coefficient and t, the time. The fuel specimens in the series I experiment have

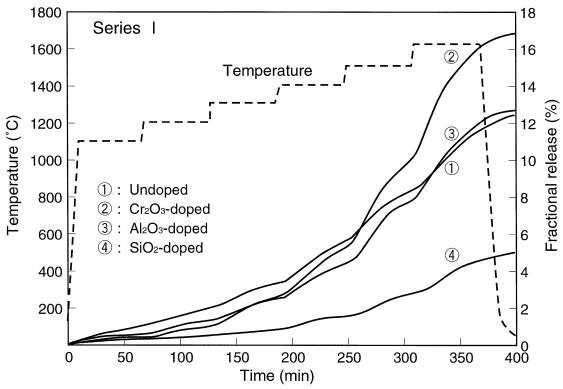

Fig. 5. Normalized cumulative fractional release of ^{133}Xe in stepwise heating test from 1100 to 1600°C (equivalent sphere radius: 1.5 μm).

slightly different equivalent sphere radii as shown in Table 3. Therefore, the fractional release values obtained from series I and II experiments were normalized to those corresponding to the equivalent sphere radii of 1.5 and 3.8 μm, respectively.

Figs. 5 and 6 show the normalized cumulative fractional release of ^{133}Xe for series I and II specimens, respectively, obtained in the stepwise heating test from 1100 to 1600°C. The total release obtained in the series I experiments (Fig. 5) becomes larger in the order: Cr_2O_3–UO_2 (16.5%) > Al_2O_3- and undoped UO_2 (12%) > SiO_2–UO_2 (4.8%). The ^{133}Xe release of the Cr_2O_3–UO_2 at high temperatures of 1500–1600°C is distinctly larger than that of undoped and Al_2O_3–UO_2 specimens. This indicates that the activation energy of ^{133}Xe diffusion for Cr_2O_3–UO_2 is larger than energies for the latter two specimens, as described in Section 3.3. By contrast, the ^{133}Xe release for the SiO_2–UO_2 specimen is the lowest among the four specimens of series I and about 1/2 of the value for the undoped UO_2 at all temperatures from 1100–1600°C. In

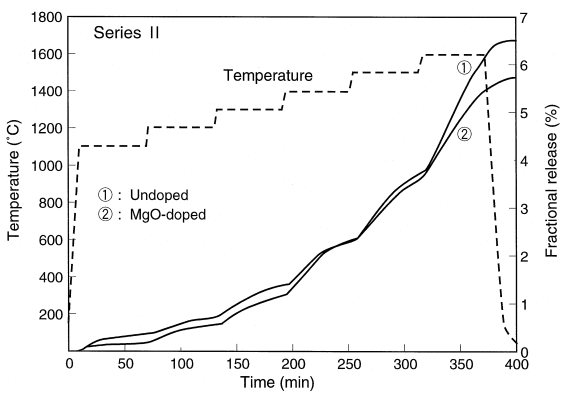

Fig. 6. Normalized cumulative fractional release of ^{133}Xe in stepwise heating test from 1100 to 1600°C (equivalent sphere radius: 3.8 μm).

the series II specimens (Fig. 6), the total release (5.7%) for MgO–UO_2 is roughly equivalent to the value (6.5%) of the undoped UO_2. Eventually, the addition of Cr_2O_3 enhances the diffusional release of ^{133}Xe and the addition of SiO_2 suppresses it. On the other hand, the additions of Al_2O_3 and MgO have no significant effect on it.

3.3. Diffusion coefficient of ^{133}Xe

The diffusion coefficient of ^{133}Xe for specimens annealed according to the stepwise pattern from 1100–1600°C can be calculated from the least squares fitted gradient of $36D/(a^2\pi)$ obtained by the F^2–t plot of Eq. (3) [2]. In this calculation, 1100°C data were excluded, because these were not in good fitness due to a small amount of ^{133}Xe release.

The temperature dependence of diffusion coefficient was evaluated from the fractional ^{133}Xe release curves on the stepwise annealing for series I and II (Figs. 5 and 6) and the equivalent sphere radii of the specimens (Table 3). The results for the five specimens are shown in Fig. 7, as a function of the inverse of absolute temperature. In Fig. 7, the values of diffusion coefficient for the four kinds of pellets obtained from the series I experiment and the values for MgO–UO_2 pellet from the series II experiment are given. The scatter in the two diffusion coefficients for undoped UO_2 was within ±20%. The solid lines in Fig. 7 were obtained by least squares fitting of the data. The diffusion coefficient lines for undoped and additive (Nb_2O_5

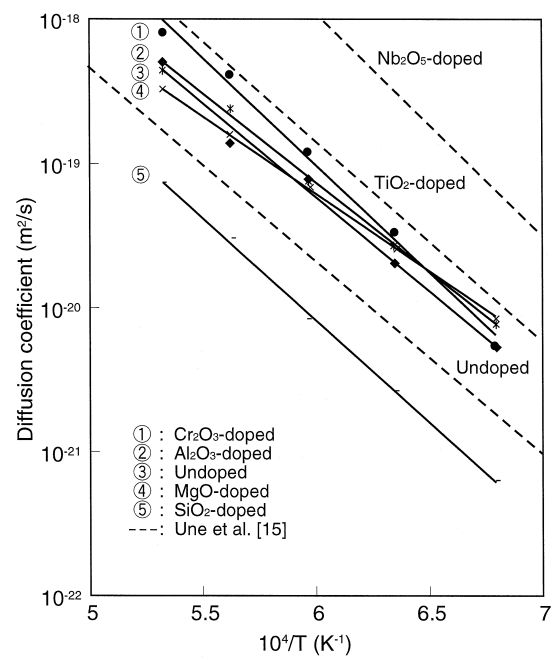

Fig. 7. Arrhenius plots of effective diffusion coefficient of ^{133}Xe against $1/T$.

or TiO_2)-doped UO_2 reported by Une et al. [15] are also shown as the dotted lines in Fig. 7. These fuel specimens were irradiated under a similar condition as in the present study. Their results showed that the addition of Nb_2O_5 and TiO_2 enhanced the diffusion coefficient of ^{133}Xe by the factors of 50 and 7, respectively. The diffusion coefficients for the present five types of specimens in the temperature range of 1200–1600°C can be classified into the following three categories.

(i) The values of the diffusion coefficient for the insoluble Al_2O_3-doped UO_2 and the soluble MgO-doped UO_2 (dissolved concentration: 0.08 wt%) are almost equivalent to that of the undoped UO_2. The diffusion coefficients for these three specimens are approximated by

$$D\,(\mathrm{m^2/s}) = 1.7\times10^{-12}\exp(-235\,(\mathrm{kJ/mol})/RT). \quad (4)$$

The scatter of the data is within ±30%, relative to Eq. (4). The values of diffusion coefficient for the undoped UO_2 obtained in the present study is about three times larger than the values reported by Une et al. [15] in the temperature range of 1200–1600°C. Compared to their activation energy of 264 kJ/mol, the present energy is slightly smaller, by about 30 kJ/mol. This difference in diffusion coefficient for undoped UO_2 is probably due to a difference in the annealing pattern. Namely, in the present experiments, a stepwise annealing pattern (annealing time: 1 h) was used, while Une et al.'s experiments adopted a one-step annealing (12 h). Furthermore, delicate distinctions during the specimen preparation and irradiation may affect the diffusion coefficients for undoped UO_2 in the two experiments.

(ii) The diffusion coefficient for the soluble Cr_2O_3-doped UO_2 (dissolved concentration: 0.012 wt%) is about three times larger than the values for the undoped UO_2 at high temperatures of 1500–1600°C, and is expressed by

$$D\,(\mathrm{m^2/s}) = 1.5\times10^{-10}\exp(-293\,(\mathrm{kJ/mol})/RT). \quad (5)$$

In Eq. (5), both the pre-exponential term and the activation energy are higher than those of Eq. (4) for the undoped, Al_2O_3- and MgO–UO_2 specimens. This activation energy is the highest among the present five specimens.

(iii) The diffusion coefficient for the soluble SiO_2-doped UO_2 (dissolved concentration: 0.045 wt%) is nearly one order of magnitude smaller than that of the undoped UO_2 in the temperature range of 1200–1600°C and is expressed by

$$D\,(\mathrm{m^2/s}) = 4.4\times10^{-12}\exp(-279\,(\mathrm{kJ/mol})/RT). \quad (6)$$

The activation energy of Eq. (6) is higher by about 40 kJ/mol, compared to the value of the undoped UO_2.

4. Discussion

From the present annealing experiments, the following two important findings have been derived. (1) The insoluble additive of Al_2O_3 has no influence on the ^{133}Xe diffusion and (2) the soluble additives of Cr_2O_3, SiO_2 and MgO have different effects, showing enhancement, suppression and no influence, respectively. Then, the reason of these effects is qualitatively interpreted in terms of the lattice defect equilibrium model in UO_2 whereby small amounts of additives with various valences are being dissolved.

Fission gas diffusion in the UO_2 lattice at low gas concentrations has been reported to proceed via an electrically neutral trivacancy which consists of a uranium vacancy, V_u, and two oxygen vacancies, V_o, according to the detailed lattice structural analysis done by Matzke [2,14]. Furthermore, theoretical calculations on lattice strain energy [20,21] have also suggested different equilibrium sites for Xe atoms, depending on fuel stoichiometry: neutral trivacancies, charged tetravacancies, divacancies or even simple cation vacancies. Comparison of the self-diffusion coefficients of oxygen and uranium ions in UO_2, shows the former to be much larger than the latter [22]. Accordingly, fission gas atom diffusion is rate-controlled by cation diffusion. Namely, the diffusion coefficient of Xe is in proportion to the concentration of uranium vacancies, which depends significantly on the concentration and valence of dissolved foreign cations and the deviation from stoichiometry (O/M ratio) [2,14].

For the Cr_2O_3-doped UO_2, the concentration of dissolved Cr_2O_3 in the UO_2 matrix was estimated to be about 0.012 wt% (0.021 at.%) based on chemical analyses, EPMA and TEM examinations. Assuming that Cr atoms enter interstitial sites in the UO_2 lattice and are ionized to a trivalency of +3, the lattice defect equilibrium is expressed by

$$2Cr_i^{*} + 3/2O_2(\mathrm{gas}) \Leftrightarrow 2Cr_i^{3+} + 3O_i^{2-}, \quad (7)$$

where Cr_i^{*} is a neutral Cr atom at an interstitial site, and Cr_i^{3+} and O_i^{2-} represent their charged interstitial ions. The estimated concentration of dissolved Cr_2O_3 of 0.021 at.% (2.1×10^{-4}) is much larger than the equilibrium defect concentration at the uranium sub-lattice in stoichiometric UO_2 ($\fallingdotseq10^{-10}$) at 1600°C [23]. Accordingly, from an electro-neutrality balance, the concentration of O_i^{2-} interstitials is approximated by

$$[O_i^{2-}] \fallingdotseq 3/2[Cr_i^{3+}], \quad (8)$$

where [ ] represents the concentration of each defect. When considering the Frenkel and Schottky equilibria, the following equations hold in the three kinds of defects of O_i, V_o and V_u:

$$[O_i][V_o] = K_1 \quad (\text{anion Frenkel defects}), \quad (9)$$

$$[V_o]^2[V_u] = K_2 \quad (\text{Schottky defects}), \quad (10)$$

where K_1, K_2 are the equilibrium constants for the reactions of the defects. Eventually, the uranium vacancy concentration of $[V_u]$ is expressed by

$$[V_u] = (3/2)^2 (K_2/K_1^2) [Cr_i^{3+}]^2. \quad (11)$$

Thus, by dissolving Cr_i^{3+} ions into the UO_2 lattice, fission gas diffusivity in Cr_2O_3–UO_2 would be enhanced through an increased V_u concentration. In this study, the diffusion coefficient of ^{133}Xe for Cr_2O_3–UO_2 at high temperatures of 1500–1600°C was increased by a factor of three, compared to the value of the undoped UO_2.

For the SiO_2–UO_2 with dissolved SiO_2 of about 0.045 wt% (0.20 at.%), the fission gas diffusion was suppressed. The diffusion coefficient of ^{133}Xe is about one order of magnitude smaller than that for the undoped UO_2, as shown in Fig. 7. In order to explain this suppression, substitutional Si_U^{2+} ions for U^{4+} in UO_2 lattice may be suggested, yielding an increased concentration of V_o. In this situation, electro-neutrality is approximated as $[V_o] \fallingdotseq [Si_U^{2+}]$. Finally, $[V_u]$ is expressed by

$$[V_u] = K_2/[Si_U^{2+}]^2. \quad (12)$$

According to Eq. (12), the uranium vacancy concentration decreases inversely with the square of the dissolved SiO_2 concentration, which may bring about lower fission gas diffusivity.

For the MgO–UO_2 with dissolved MgO of 0.08 wt% (0.54 at.%), MgO is not only dissolved in the UO_2 lattice, but also dispersed in the grain interiors as small precipitates of 9 nm in size (Fig. 3); nevertheless the diffusional fission gas release was not affected. MgO can be dissolved to higher concentrations of 25–39 at.% [24–27] at higher oxygen potentials, i.e. in hyperstoichiometric $(U, Mg)O_{2+x}$. However, at lower oxygen potentials, its solubility becomes lower, about 0.2 at.% at 1750°C [28] or 0.8 at.% at 1700°C [11,13]. The dissolved MgO concentration (0.54 at.%) in the present specimen is in the middle of the above values. As a defect structure, substitution of Mg^{2+} ions for U^{4+} ions has been proposed [29]. The O/M ratio of the present MgO–UO_2 is very close to the stoichiometric composition of 2.00. In this situation, it may be expected that the electro-neutrality balance in the crystal is kept by oxidizing U^{4+} ions to U^{5+} ions, rather than yielding oxygen vacancies [29]. According to this defect equilibrium, the dissolution of MgO has no effect on uranium vacancy concentration and, therefore, no effect on fission gas release diffusivity. In an irradiation test up to 28 GWd/t, the fission gas release from 0.75 wt% MgO–UO_2 pellets (grain size: 35 μm) was reduced by a factor of > 2.5, in comparison with the value from undoped UO_2 pellets (4 μm) [11,13]. This suppression is possibly attributed to a grain size effect because of the longer diffusion distance in the former pellets, although the authors themselves suggested a reduced fission gas diffusivity for the MgO–UO_2.

In the present MgO–UO_2 specimen, which was annealed in a reducing atmosphere, a large number of small MgO precipitates (9 nm in size) are dispersed in the grain interiors. Their estimated amount is about 0.38 wt%. The defect clusters, small precipitates and grain boundaries would act as trapping sites for fission gases [2]. Then, the effect of small MgO precipitates on fission gas diffusion was theoretically assessed. The mean diameter, d, and number density, N, of MgO precipitates are 9 nm and 3×10^{22} m^{-3} from TEM observation (Fig. 3). The mean separation for regularly arranged precipitates in a simple cubic lattice is about 30 nm, which was calculated from the relationship $d = N^{-1/3}$. Based on the diffusion theory, the root-mean-square movement of fission gas atoms, λ, is given by

$$\lambda = (4Dt)^{1/2}. \quad (13)$$

For example, for a 1600°C × 1 h heating, λ is about 90 nm using the value of D obtained in this study. In this situation, fission gas atoms go through only 2–3 layers of regularly arranged MgO precipitates in the UO_2 matrix, thus the collision trapping effect of fission gas atoms by small precipitates is not so significant. A geometrical collision probability, P, of fission gas atoms with particles (radius: R) is expressed by [30]

$$P = 4\pi RND. \quad (14)$$

Substituting the measured R, N and D into Eq. (14), P at 1600°C is about 1×10^{-3} s^{-1}. When the total volume of precipitates, V, is constant, N is given by

$$N = 3V/4\pi R^3. \quad (15)$$

Thus, the collision probability is inversely proportional to the square of R. By reducing the MgO particle size to 1–2 nm, which may be feasible by controlling the sintering and annealing conditions of MgO–UO_2 pellet, the collision probability will be increased by a factor of about 100 and fission gas diffusivity in the UO_2 matrix may be remarkably reduced.

5. Conclusions

From post-irradiation annealing experiments at 1100–1600°C, the effect of small amounts of additives (0.065 wt% Cr_2O_3, 0.076 wt% Al_2O_3, 0.085 wt% SiO_2 and 0.50 wt% MgO) on the diffusional release of ^{133}Xe from UO_2 fuels was examined. The conclusions obtained in this study are as follows.

(1) For the Cr_2O_3- and SiO_2–UO_2 fuel pellets, which were sintered in a reducing atmosphere of H_2 at 1750°C for 2 h, their dissolved concentrations were analyzed as 0.012 and 0.045 wt%, respectively. On the other hand, the Al_2O_3–UO_2 pellet, which was prepared by the same procedure, had no additive solubility. For the MgO–UO_2

pellet, a special preparation process was adopted: First the powder compact was sintered in a slightly oxidizing atmosphere of Ar at 1660°C for 2 h and then annealed in a reducing atmosphere ($N_2 + 8\%$ H_2, dew point 20 and -35°C) at 1660°C for 2 h. The dissolved concentration of MgO was 0.08 wt%. In this pellet, a large number of small MgO precipitates of 9 nm in size were uniformly dispersed in the grains.

(2) The diffusion coefficients for the present five types of specimens in the temperature range of 1200–1600°C could be classified into the following three categories.

(i) The values of the diffusion coefficient for the insoluble Al_2O_3-doped UO_2 and the soluble MgO-doped UO_2 were almost the same as the value of the undoped UO_2. The dissolved MgO and small MgO precipitates (9 nm) had almost no influence on fission gas diffusion. The diffusion coefficients for these three specimens were approximated by

$$D\ (\mathrm{m^2/s}) = 1.7 \times 10^{-12} \exp(-235\ (\mathrm{kJ/mol})/RT).$$

(ii) The diffusion coefficient for the soluble Cr_2O_3-doped UO_2 was about three times larger than the value for the undoped UO_2 at high temperatures of 1500–1600°C and was given by

$$D\ (\mathrm{m^2/s}) = 1.5 \times 10^{-10} \exp(-293\ (\mathrm{kJ/mol})/RT).$$

(iii) The diffusion coefficient for the soluble SiO_2-doped UO_2 was nearly one order of magnitude smaller than that of the undoped UO_2 in the temperature range of 1200–1600°C and was expressed by

$$D\ (\mathrm{m^2/s}) = 4.4 \times 10^{-12} \exp(-279\ (\mathrm{kJ/mol})/RT).$$

(3) The different effects of the dissolved additives on ^{133}Xe diffusivity were qualitatively interpreted in terms of the diffusion model of fission gas atoms via vacancy clusters and the lattice defect equilibrium model in the UO_2 lattice.

Acknowledgements

The authors would like to express their gratitude to Mr K. Nogita for carrying out TEM observations and to Mr A. Hanawa for EPMA examinations.

References

[1] G.T. Lawrence, J. Nucl. Mater. 71 (1978) 195.
[2] Hj. Matzke, Radiat. Eff. 53 (1980) 219.
[3] T. Kubo, T. Hosokawa, R. Yuda, K. Une, S. Kashibe, K. Nogita, Y. Shirai, H. Harada, T. Kogai, T. Kubo, J.H. Davies, Proc. Int. Topical Meeting on Light Water Reactor Fuel Performance, West Palm Beach, Florida, 1994, p. 650.
[4] K.C. Radford, J.M. Pope, J. Nucl. Mater. 116 (1983) 305.
[5] P.T. Sawbridge, G.L. Reynolds, B. Burton, J. Nucl. Mater. 97 (1981) 300.
[6] J.B. Ainscough, F. Rigby, S.A. Marrow, J. Am. Ceram. Soc. 64 (1981) 315.
[7] J.C. Killeen, J. Nucl. Mater. 58 (1975) 39.
[8] H. Assmann, W. Dorr, G. Gradel, G. Maier, M. Peehs, J. Nucl. Mater. 98 (1981) 216.
[9] J.B. Ainscough, F. Rigy, S.C. Osborn, J. Nucl. Mater. 52 (1974) 191.
[10] J.C. Killeen, J. Nucl. Mater. 88 (1980) 177.
[11] P.T. Sawbridge, C. Baker, R.M. Cornell, K.W. Jones, D. Reed, J.B. Ainscough, J. Nucl. Mater. 95 (1980) 119.
[12] P.L. Allen, J.B. Ainscough, N. Beatham, R.H. Watson, BNES Conf. on Gas Cooled Reactor Today, Paper 65, BNES, London, 1982.
[13] B.E. Ingleby, K. Hand, Proc. on Fission Product Behavior in Ceramic Oxide Fuel, Am. Ceram. Soc., Adv. Ceram. 17 (1986) 57.
[14] Hj. Matzke, Nucl. Appl. 2 (1966) 131.
[15] K. Une, I. Tanabe, M. Oguma, J. Nucl. Mater. 150 (1987) 93.
[16] K. Une, S. Kashibe, K. Ito, J. Nucl. Sci. Technol. 30 (1993) 221.
[17] T. Fujino, J. Tateno, H. Tagawa, J. Solid State Chem. 24 (1978) 11.
[18] K. Shiba, A. Itoh, M. Akabori, J. Nucl. Mater. 126 (1984) 18.
[19] S.M. Lang, F.P. Knudsen, C.L. Fillmore, R.S. Roth, High-Temperature Reactions of Uranium Dioxide with Various Metal Oxides, 20 Feb. 1956, NBS Circ. 568.
[20] R.A. Jackson, C.R.A. Catlow, J. Nucl. Mater. 127 (1985) 161.
[21] R.W. Grimes, in: S.E. Donnelly, J.H. Evans (Eds.), Fundamental Aspects of Inert Gases in Solid, Plenum, New York, 1991, p. 415.
[22] Hj. Matzke, J. Chem. Soc. Faraday Trans. 86 (1990) 1243.
[23] Hj. Matzke, J. Nucl. Mater. 114 (1983) 121.
[24] J.S. Anderson, K.D.B. Johnson, J. Chem. Soc. (1953) 1731.
[25] T. Fujino, K. Naito, J. Inorg. Nucl. Chem. 32 (1970) 627.
[26] R.P. Budnikov, S.G. Tresystsky, V.I. Kushokovsky, 2nd Geneva Conf., vol. 6, 1958, p. 127.
[27] M. Sugisaki, K. Hirashima, S. Yoshihara, Y. Oishi, J. Nucl. Sci. Technol. 10 (1973) 387.
[28] J.B. Ainscough, F. Rigby, J. Inorg. Nucl. Chem. 36 (1974) 1531.
[29] M. Sugisaki, J. Nucl. Mater. 79 (1979) 338.
[30] D. Olander, Fundamental Aspects of Nuclear Reactor Fuel Elements, TID26711-P, 1976, pp. 287–332.